

## RESEARCH ARTICLE

# Bright ultrashort echo time SWIFT MRI signal at the osteochondral junction is not located in the calcified cartilage

Olli Nykänen<sup>1</sup>  | Henri P. P. Leskinen<sup>1</sup>  | Mikko A. J. Finnilä<sup>1,2</sup>  |  
Sakari S. Karhula<sup>2,3</sup> | Mikael J. Turunen<sup>1,4</sup>  | Juha Töyräs<sup>1,5,6</sup>  |  
Simo Saarakkala<sup>2,3</sup>  | Mikko J. Nissi<sup>1,2</sup> 

<sup>1</sup>Department of Applied Physics, University of Eastern Finland, Kuopio, Finland

<sup>2</sup>Research Unit of Medical Imaging, Physics and Technology, University of Oulu, Oulu, Finland

<sup>3</sup>Department of Diagnostic Radiology, Oulu University Hospital, Oulu, Finland

<sup>4</sup>SIB Labs, University of Eastern Finland, Kuopio, Finland

<sup>5</sup>Diagnostic Imaging Center, Kuopio University Hospital, Kuopio, Finland

<sup>6</sup>School of Information Technology and Electrical Engineering, The University of Queensland, Brisbane, Australia

## Correspondence

Olli Nykänen, Department of Applied Physics, University of Eastern Finland, POB 1627, FI-70211 Kuopio, Finland.  
Email: [olli.nykanen@uef.fi](mailto:olli.nykanen@uef.fi)

## Funding information

Academy of Finland, Grant/Award Numbers: #285909, #293970, #319440; Finnish Cultural Foundation, Grant/Award Number: #00180787; North-Ostrobothnia regional fund of Finnish Cultural Foundation, Grant/Award Number: #60172246

## Abstract

In this study, we aimed to precisely localize the hyperintense signal that is generated at the osteochondral junction when using ultrashort echo time magnetic resonance imaging (MRI) and to investigate the osteochondral junction using sweep imaging with Fourier transformation (SWIFT) MRI. Furthermore, we seek to evaluate what compositional properties of the osteochondral junction are the sources of this signal. In the study, we obtained eight samples from a tibial plateau dissected from a 68-year-old male donor, and one additional osteochondral sample of bovine origin. The samples were imaged using high-resolution ultrashort echo time SWIFT MRI and microcomputed tomography ( $\mu$ CT) scans. Localization of the bright signal in the osteochondral junction was performed using coregistered data sets. Potential sources of the signal feature were examined by imaging the bovine specimen with variable receiver bandwidths and by performing variable flip angle T1 relaxation time mapping. The results of the study showed that the hyperintense signal was found to be located entirely in the deep noncalcified articular cartilage. The intensity of this signal at the interface varied between the specimens. Further tests with bovine specimens indicated that the imaging bandwidth and T1 relaxation affect the properties of the signal. Based on the present results, the calcified cartilage has low signal intensity even in SWIFT imaging. Concomitantly, it appears that the bright signal seen in ultrashort echo time imaging resides within the noncalcified cartilage. Furthermore, the most likely sources of this signal are the rapid T1 relaxation of the deep cartilage and the susceptibility-induced effects arising from the calcified tissues.

## KEYWORDS

cartilage, osteochondral junction, subchondral bone, SWIFT, UTE

## 1 | INTRODUCTION

Osteoarthritis (OA) is a joint disease that causes severe pain, leading to restricted mobility of a patient and it cannot be reversed via medication.<sup>1-3</sup> Moreover, means to study the onset and progression

of OA are limited.<sup>3</sup> Recently, the role of the osteochondral junction, the interface between cartilage and the underlying bone, has received considerable interest in terms of its connection to the development and progression of OA.<sup>4,5</sup> Multiple degradative changes at the osteochondral junction have been linked to the progression of

This is an open access article under the terms of the Creative Commons Attribution License, which permits use, distribution and reproduction in any medium, provided the original work is properly cited.

© 2020 The Authors. *Journal of Orthopaedic Research*® published by Wiley Periodicals LLC on behalf of Orthopaedic Research Society.

the disease, for example, multiplication of the tidemark and vascular invasion into cartilage.<sup>6-11</sup>

Magnetic resonance imaging (MRI) is a widely used tool in clinical diagnostics of OA but is limited with the capability for imaging of mineralized tissues because traditional MRI techniques cannot detect signals emerging from them due to the extremely fast T2 relaxation. However, modern ultrashort echo time (UTE) sequences can catch these rapidly decaying signals and thus they may be used in the imaging of the osteochondral junction. Earlier, a bright signal from the osteochondral junction has been observed using different UTE sequences.<sup>12-15</sup> In a study with 2D dual inversion prepared UTE sequence (DIR-UTE), it was shown that the signal has contributions from the deepest parts of hyaline cartilage and from the calcified cartilage. Another study using same the sequence revealed the same signal from cartilaginous endplates.<sup>16</sup> One study applying DIR-UTE reported that this signal has T2\* relaxation time around 2 milliseconds, T1rho around 3.5 milliseconds and T1 around 300 milliseconds.<sup>15</sup> A study incorporating sweep imaging with Fourier transformation (SWIFT) sequence showed that similar signal can also be seen using 3D SWIFT MRI.<sup>14</sup> Furthermore, the defects in this hyperintense signal, as observed with 3D UTE, appear to co-locate with bone marrow lesions.<sup>17</sup>

While the calcified cartilage and deep cartilage together were suggested as potential sources, precise origin of the bright signal is yet unclear. Due to the significance of the cartilage-bone interface in the disease progression,<sup>7,9</sup> our aim was to precisely locate this signal, and investigate which compositional properties could potentially cause it. We propose the use of SWIFT sequence,<sup>18</sup> which, as a zero echo time method has equal ability to capture the same signal seen in UTE imaging and enables high-resolution 3D imaging which further allows precise coregistration between MRI and microcomputed tomography ( $\mu$ CT) images. As it is likely that the signal is altered during degeneration of the cartilage, precise localization is critical in resolving what degradative processes could affect the signal.

We hypothesize that the signal does not emerge directly from the calcified cartilage, but is instead caused by the shorter T1 relaxation in the deep cartilage and the rapid change in magnetic susceptibility at the boundary between the noncalcified and calcified cartilage, features which have both been demonstrated earlier.<sup>19-22</sup>

To test the hypothesis, we obtained high-resolution SWIFT<sup>18</sup> scans of human and bovine osteochondral samples at 9.4 T and the resulting 3D MR images were compared with both high-resolution 3D  $\mu$ CT data as well as histological images of the same samples.

## 2 | METHODS

### 2.1 | Samples

Cylindrical (diameter = 4 mm) osteochondral samples ( $n = 8$ ) were obtained from human cadaver tibia. The samples were harvested

from different sites of the tibia, four from the lateral and four from the medial side. The samples were stored in the freezer quickly after harvesting and stored there until MRI. Collection of the samples was approved by the Research Ethics Committee of Northern Savo Hospital District, Finland (approvals no. 58/2013 and 134/2015). One of the samples had to be rejected from the final data set due to severe motion artifacts caused by the sample floating away from its position in perfluoropolyether during the scan. Since the SWIFT image reconstruction is done off-line, the sample had already been passed on to other studies at the time this was discovered. Additionally, a bovine osteochondral sample was imaged to allow for more time-consuming studies of the signal at the osteochondral junction. The bovine sample was utilized since the limited availability of scanner time together with the limited availability of the samples severely restricted the allowed imaging time for the human samples (the same samples were used in a subsequent time-critical study).

### 2.2 | Measurements

MRI was performed at 9.4 T with Varian/Agilent scanner (VnmrJ DirectDrive software v.3.10) using a 10-mm diameter quadrature RF volume transceiver (Rapid Biomedical GmbH, Rimpar, Germany). The samples were immersed in <sup>1</sup>H MRI signal-free perfluoropolyether inside a plastic test tube. Samples were oriented in such a way that the surface of the cartilage was perpendicular to the main magnetic field of the scanner, that is, approximately the same orientation tibial cartilage would have in *in vivo* conditions. SWIFT data were acquired using gapped hyperbolic secant pulse, a bandwidth of 62.5 kHz, flip angle of 6°, a field of view of 2.5 cm, and image dimensions of 384 × 384 × 384 voxels. The number of radial spokes per image was 262 144 and the images were reconstructed using re-gridding on a Cartesian grid. SWIFT images were obtained by separately applying fat saturation, water saturation, short T2\* saturation, or no saturation. The short T2\* saturation was based on the principle that the spectral width of the short T2\* species is larger than that of longer T2\* spins and thus saturation of the short T2\* species could be achieved by applying spectral saturation that was far enough from water and fat resonance frequencies. The spectral saturation was done by applying 20-millisecond 180° hyperbolic secant pulses with 1 kHz bandwidth at a specified offset frequency ( $\pm 1400$  kHz) after every 16<sup>th</sup> spoke. In the data set without saturation, the corresponding time delay was applied at the same points. Data sets without saturation pulses were also collected using variable flip angles to perform T1 relaxation time mapping.<sup>22,23</sup> After the MRI scans, high-resolution  $\mu$ CT images were acquired using a Skyscan 1272 device (Bruker microCT, Kontich, Belgium) by using X-ray tube voltage of 50 kV and 200- $\mu$ A current, and 0.5-mm aluminum filtering to collect 1200 projections with 2200-millisecond exposure time and three times frame averaging. Projections were reconstructed to images with isotropic 2.75- $\mu$ m voxel size with NRecon-software (v.1.6.10.4; Bruker microCT) utilizing beam hardening and ring artifact corrections.

### 2.3 | Data analysis

Differently saturated SWIFT images were combined to create images, where both water and fat signals were in focus (without radial blurring, *all-in-focus* images) and images showing only the short T2\* signals (*short T2\** images). The in-focus images were created by removing the water-saturated images (reconstructed at water resonance frequency) from the nonsaturated images and then adding water-saturated images reconstructed at the fat resonance frequency. Short T2\* images were calculated by subtracting short T2\* saturated images from the nonsaturated images (Figure 1).

The 3D MR images were coregistered with the 3D  $\mu$ CT images using Elastix software<sup>24</sup> to allow precise localization of the bright signal feature in the SWIFT images with respect to the bony features of the specimens. The coregistration was performed between the  $\mu$ CT images and all-in-focus MR images with inverted contrast and background masking to maximize the similarity of the contrast between the modalities to aid the automatic coregistration. Affine transform and mutual information cost function were utilized in the coregistration. Affine transform was chosen due to different imaging geometries in MRI and  $\mu$ CT. Spline transform was not utilized as it was not expected that the samples would deform between MRI and CT. The full parameter files used with Elastix can be found in the

open data set of this study. The transform parameters from the coregistration were then utilized to coregister the rest of the MR images acquired in the same geometry. In the end, success of the coregistration was confirmed visually. To perform visual inspection of the coregistration, bone boundaries were generated from the binarized  $\mu$ CT images via 3D morphological erosion and subtraction in ImageJ, and subsequently overlaid on the SWIFT images.

Custom-made Matlab algorithm was used to calculate depth-wise signal intensity profiles from both MRI and  $\mu$ CT data at the osteochondral junction. The profiles were averaged over cylindrical columns (width, 2 mm) in the middle of the specimens, and these profiles were analyzed further (Figure S1).

Histological sections were stained with Masson's trichrome<sup>25</sup> and Safranin O<sup>26</sup> and imaged with a digital pathology slide scanner ( $\times 40$  magnification and 0.25- $\mu$ m pixel size, Aperio AT2; Leica Biosystems, Wetzlar, Germany). To further assess the different structural features of the osteochondral samples and to evaluate the sources of the bright signal in SWIFT images, the microscopic images were manually matched with the  $\mu$ CT images to allow cross-modality comparison. Safranin O-stained sections were graded using Osteoarthritis Research Society International (OARS) scoring system to evaluate the progression of OA in the samples.<sup>27</sup>

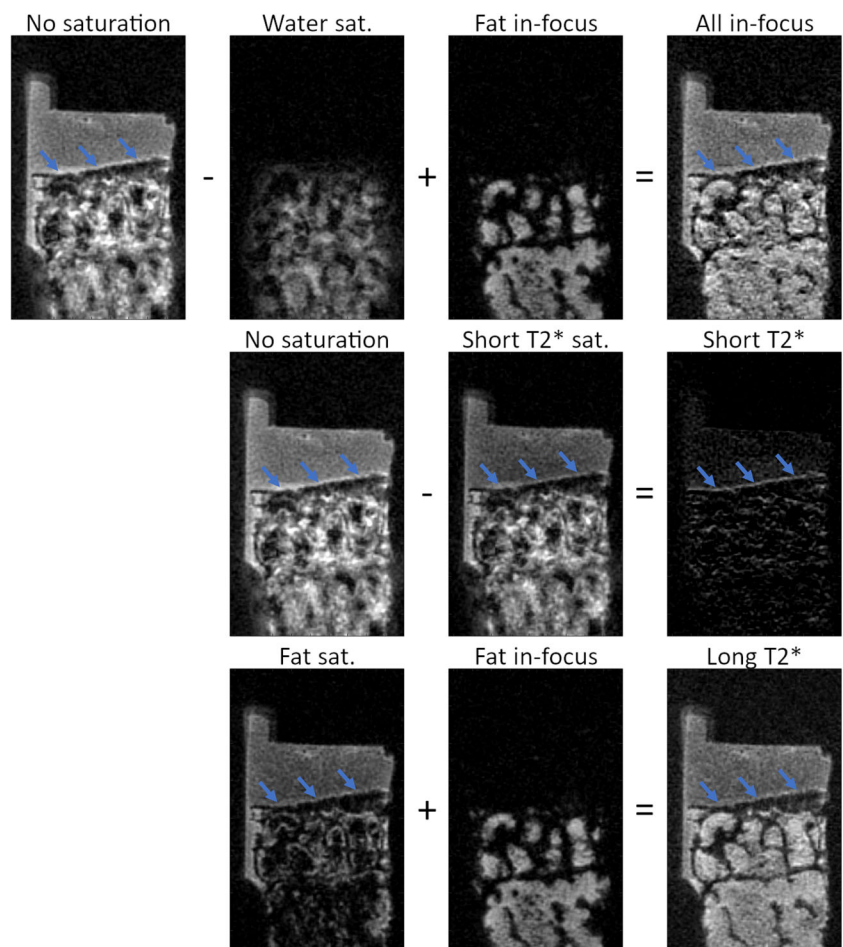


**FIGURE 1** Sweep imaging with Fourier transformation images with the different saturations and the hybrid images created by combining the saturated images. Top row: formation of all signal in-focus image, middle row: short T2\* signal-only image and bottom row: long T2\* signals only. The bright signal is visible in most of the images but is especially well seen in the short T2\* and all signals in-focus images. The bright signal is pointed out by the blue arrows

Additional correlation analysis was performed between the short T2\*/long T2\* ratio of the SWIFT signal and the intensity of the signal at the osteochondral junction and thickness and bone volume/total volume of the subchondral plate using Pearson's correlation coefficient. Due to the small sample size, the results of this analysis are descriptive and are presented only as Supporting Information Data.

### 3 | RESULTS

Creating hybrid images from the saturated images was successful and the bright signal that is present in the nonsaturated images could be preserved through the manipulations to the *all-in-focus* and *short T2\** images (Figure 1). In addition, it was evident that without the hybrid images, blurring from the bone marrow fat would have complicated the analysis (Figure 1).

The coregistration between SWIFT MRI and  $\mu$ CT was successful (Figure 2) and allowed localization of the bright signal at the osteochondral junction both visually and using average profiles through the sample (Figures 3 and 4). From the co-registered data sets, it was evident that the increase in SWIFT signal appeared spatially before anything that was visible in the  $\mu$ CT, that is, the signal originated from the noncalcified cartilage. Here, at very high  $\mu$ CT resolution, only a slight increase in the density of the calcified cartilage was observed. Thus, calcified cartilage is fully included in bone segmentation (Figure 3, Video S1). Furthermore, our results indicate that the bright signal is not located in the calcified cartilage, which remained almost invisible even in the SWIFT images. Out of the seven samples, six exhibited the bright signal at the osteochondral junction and one did not (or had a much less bright signal) (Figure 4). The bright signal was also visible in the bovine sample that was used in further investigations (Figure 5). Furthermore, the location of the bright signal appeared to move toward the osteochondral junction in the reconstructed short T2\* images as compared to the images with all the signals (Figures 4 and 5).

T1 relaxation time mapping revealed that T1 relaxation time decreases toward and through the osteochondral junction; this change is very steady through the interface and does not present any jumps near the interface (Figure 6). The proton density (S0) map from the T1 mapping data set did not display a distinct signal increase at the junction either, however, it decreased rapidly in the calcified cartilage (Figure 6). Together, the T1 and S0 data result in a steady signal increase toward the deep noncalcified articular cartilage due to the reducing T1, followed by an intensity drop at the calcified cartilage, where the proton density drops. Scans with variable imaging bandwidths showed that with lower bandwidths the bright signal becomes blurrier, its peak widens and moves away from the osteochondral junction and vice versa (Figure 5). The bandwidth test also confirmed that the peak is observed closer to the osteochondral junction in the short T2\*-only images.

The OARS scores of the samples ranged from 1.5 to 4.5 (median, 3), indicating that all samples were affected by the degradation due to OA.

### 4 | DISCUSSION

We investigated the localization and origins of the bright signal feature, which is observed at the osteochondral junction in SWIFT imaging. A few previous reports have investigated the same feature using UTE-based sequences,<sup>12,13,15</sup> however, without signal localization to reference structures based on  $\mu$ CT. In our preliminary work,<sup>14</sup> we noted that the changes in magnetic susceptibility over the interface have a likely role in the formation of the signal and this study was conducted to investigate the precise origin of the signal. We observed that the bright signal at the osteochondral junction is not located in the calcified cartilage; instead, it is in the deep noncalcified articular cartilage, although it likely has a contribution from the calcified cartilage via local field distortions due to susceptibility differences between the calcified and noncalcified tissues. The findings presented here may not be directly generalized to UTE sequence, 3D or 2D DIR-UTE as applied in many previous studies,<sup>12,13,15,16</sup> as UTE and SWIFT are inherently different sequences. However, the sequences should produce very similar data since they are both capable of detecting also the signals that decay extremely rapidly due to the associated extremely short T2\* relaxation times.

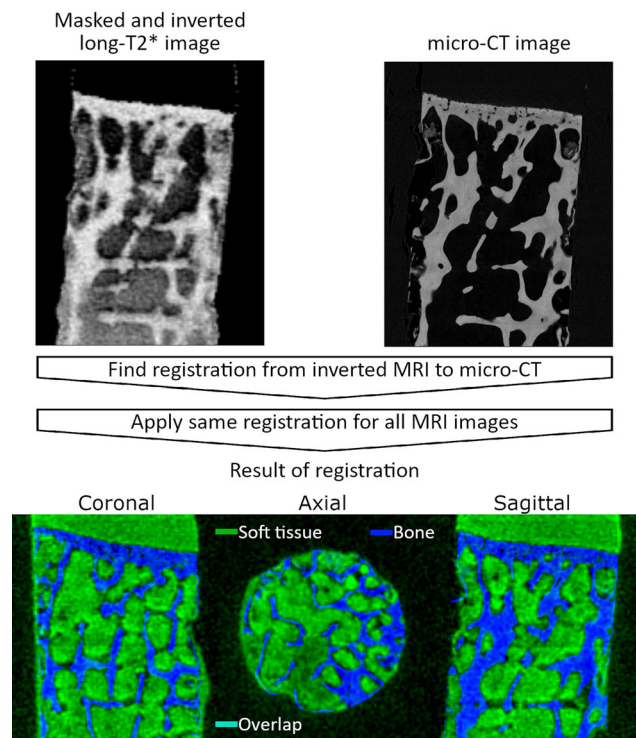


**FIGURE 2** Coregistration between magnetic resonance imaging (MRI) and microcomputed tomography ( $\mu$ CT). Green color shows the MRI intensity (ie, soft tissues such as cartilage and bone marrow fat) and blue the  $\mu$ CT image intensity (ie, bony structures). The overlap of the signals is displayed as cyan color. Coregistration was highly successful with very limited overlap of the signals (minimal amount of cyan-colored regions visible)

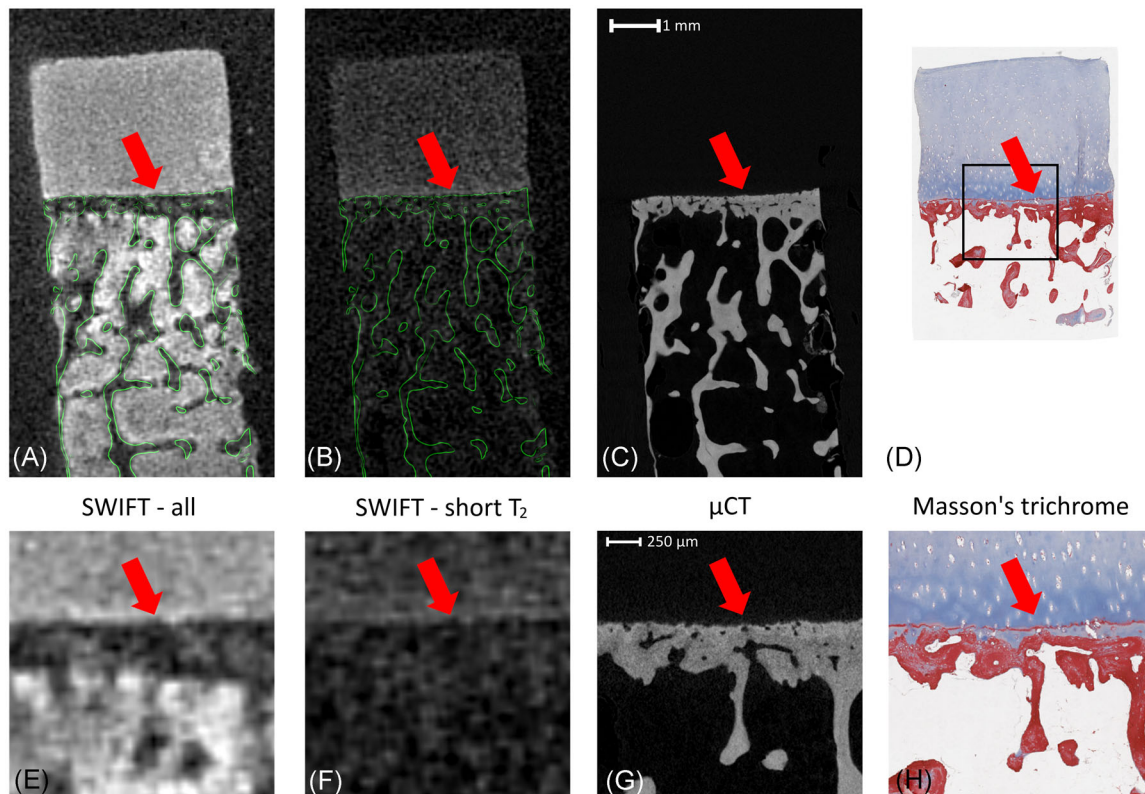


**FIGURE 3** Example images from the different imaging modalities. (A) SWIFT (sweep imaging with Fourier transformation) image with water and fat signals in focus, (B) SWIFT image with short T2\* signals only, (C) microcomputed tomography (μCT) image, (D) Masson's trichrome-stained histological slice from the same specimen. On the bottom row, magnifications of a region at the osteochondral junction are presented; (E) SWIFT image with water and fat signal in focus, (F) SWIFT image with short T2\* signals only, (G) μCT image and (H) Masson's trichrome stained histological slice. The SWIFT images on the top row show the outline of the trabecular bone generated from the μCT data, confirming the coregistration match. Red arrows point to the location of the bright MRI signal. Light microscopic image of Masson's trichrome-stained sections shows the bone in red, calcified cartilage on top of the bone followed by the tidemark line shown in red and the noncalcified cartilage. The calcified cartilage in μCT exhibits similar attenuation to bone

Coregistrations were deemed highly successful. The coregistration between SWIFT MRI and μCT images confirmed that the bright signal in MRI is almost entirely located in the regions that are not visible in μCT images and vice versa, the x-ray attenuation ramps up only after the MRI signal vanishes (Figures 3-6). Moreover, careful matching between the μCT and histological slices as well as our previous results with low-resolution μCT<sup>28</sup> confirm that calcified cartilage is visible in μCT images, that is, *seen as bone* (Figure 3; Supporting Information Data). Thus, it can be concluded that the bright signal in SWIFT MRI is *not directly located in the calcified cartilage*. However, it is likely (and also suggested by the variable bandwidth experiments, see discussion below) that this signal contains some information about the subchondral plate and even from the entire osteochondral unit, as it has been observed that lack of this signal colocalizes with bone marrow lesions.<sup>17</sup>

The measurements showed that the T1 relaxation time decreases toward the osteochondral junction, which is in line with previous studies.<sup>21,22</sup> This *partially* explains the observed signal increase at the osteochondral junction. T1 relaxation time decreases in the deep cartilage likely due to the increase in solid

fraction toward the deep cartilage.<sup>29,30</sup> If the signal modulation in the deep cartilage is mainly caused by the T1 relaxation, it has probably remained unseen in the conventional MRI scans due to the fact that in the common sequences, the extremely fast T2(\*) relaxation dominates the signal in the deep cartilage and near the osteochondral junction, whereas in the UTE sequences, T2\* effects are minimal. Instead, the T1 and proton density dominate the signal in the UTE sequences.

We also observed that a decrease in the imaging bandwidth leads to a decrease in the relative intensity of the bright signal feature and blurring of the signal. Furthermore, the peak of the bright signal seemed to move away from the osteochondral junction when the imaging bandwidth was lowered. Since the imaging bandwidth changes the appearance of the signal, it can be deduced that the signals at the osteochondral junction do not have the same Larmor frequencies as the rest of the signal in the noncalcified articular cartilage, indicating that susceptibility change (from hyaline cartilage to calcified tissues, ie, calcified cartilage and bone<sup>31</sup>) at the osteochondral junction plays a role in the formation of the bright signal feature. In the present samples, the maximum intensity seemed to

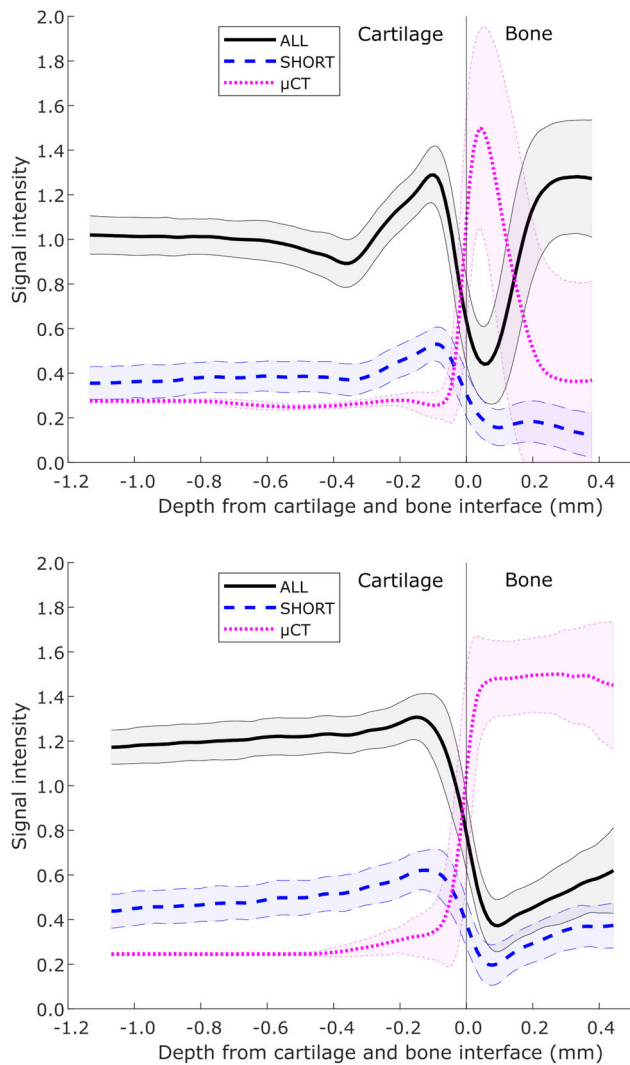


**FIGURE 4** Normalized magnetic resonance imaging (MRI) intensities and X-ray absorption nearby the osteochondral junction (noncalcified-calcified tissue interface). The profiles show that the intensity of the signal at the osteochondral junction varied clearly. Top: sample with a high-intensity signal at the interface. Bottom: sample with a distinctly lower signal at the interface. The profiles also demonstrate that the bright signal is located next to the bony tissues at the interface

shift toward interface in the short T2\* images, which hints that the hyperintense signal is not only caused by the fast relaxing spins but it also has contributions from other signal elements, such as faster T1 relaxation close to the osteochondral junction.

With the samples of the present study, the biological significance of the signal at the interface cannot be conclusively investigated. An earlier report by Bae et al<sup>13</sup> showcased an osteochondral specimen exhibiting degenerative features and noted that the bright signal depends on the properties of the specimen and its degenerative status. It is known that the calcification front advances in degeneration<sup>7,9</sup> and thus results in changes in the magnetic susceptibility of the deep cartilage. Furthermore, the underlying bony structures undergo changes<sup>4,28</sup> during degeneration,

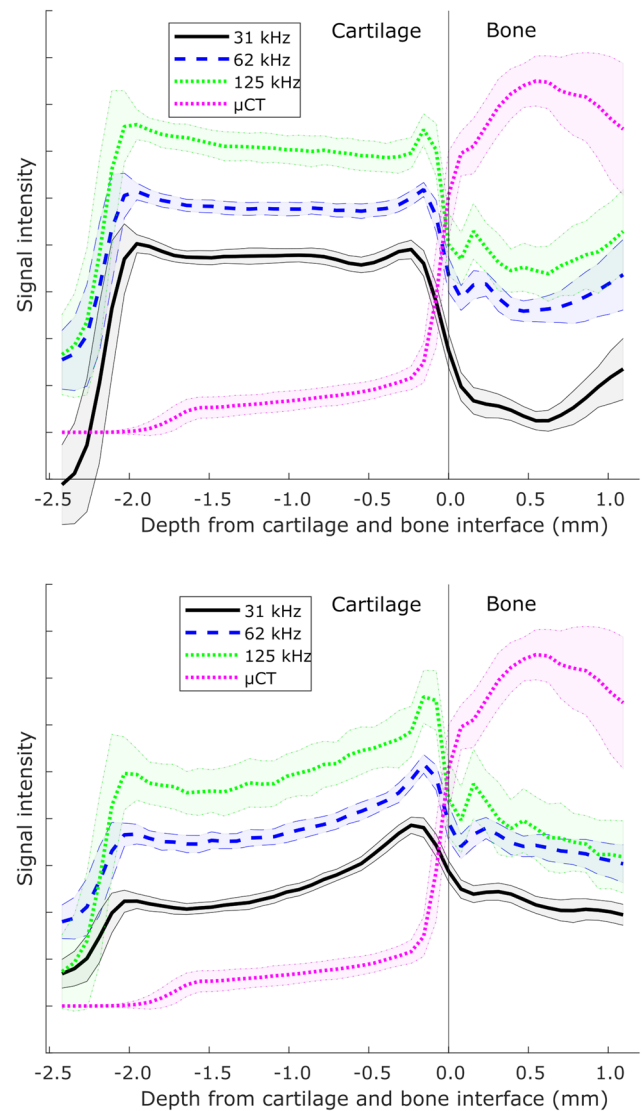


**FIGURE 5** Normalized magnetic resonance imaging intensities and X-ray absorption nearby the osteochondral junction in the bandwidth test for both all signal (top) and short T2\* signal (bottom). The bright signal feature becomes sharper and more intense with higher imaging bandwidths. Also, the peak signal shifts toward interface in the short T2\* profiles

further modifying the magnetic tissue properties around the interface. The characteristics of the bright signal varied between the samples (Figure 4), suggesting that the signal may be related to physiological processes that occur at the osteochondral junction. Additional correlation analysis (Figure S2) indicated that the signal from the osteochondral junction may provide information on the thickness and porosity of the subchondral plate. However, correlation results are merely directional due to the small sample size and further studies are required to elucidate the diagnostic potential of the SWIFT sequence at the osteochondral junction. Taken together, it is reasonable to assume that the SWIFT signal at the osteochondral junction depends on the degenerative status of the different tissues in the osteochondral unit, providing an attractive

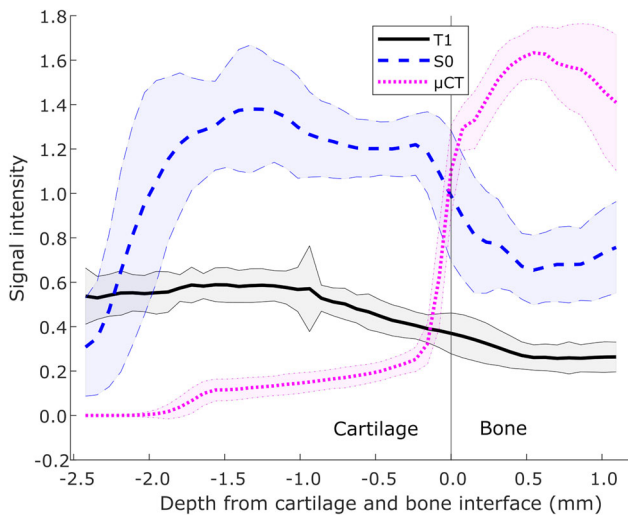


**FIGURE 6** Normalized T1 relaxation time and proton density (S0) from T1 mapping along with  $\mu$ CT x-ray absorption. T1 decreases toward the interface. In S0, the peak nearby the interface is less intense than that of the measured signal, pointing out that decreasing T1 relaxation plays a role in the formation of the bright signal

window into MR imaging of the degenerative changes in tissues that are not visible with standard MRI sequences.

There are several limitations in the study. Firstly, the sample size was small ( $n = 7$ ) and comparison between healthy and degenerated cartilage could not be performed due to that. Moreover, all samples were degenerated at least slightly based on the OARSI grading. Secondly, *in vivo* translatability of the technique is limited due to the lack of the SWIFT sequence on most of the clinical scanners and the high-resolution demand for the analysis. However, similar measurements can be performed using other UTE or zero echo time sequences<sup>32,33</sup> that are more widely available. Finally, as many of the MRI parameters have demonstrated orientation dependence in articular cartilage,<sup>14,34</sup> the bright signal feature could also be studied at multiple orientations. This was, however, not possible with the cadaveric samples of the study due to logistic reasons.

In conclusion, we found that the bright signal observed at the osteochondral junction in SWIFT imaging does not localize in the calcified cartilage, which has low signal also in SWIFT images. Instead, this signal is found in the noncalcified cartilage above the calcified tissues. Furthermore, rapid T1 relaxation appears to have a role in the formation of the signal. The susceptibility differences between the noncalcified cartilage and calcified tissues are also potential contributors to the signal. As this bright signal feature depends on the properties of the tissue, UTE sequences likely have diagnostic potential for OA imaging, as they allow sensitive imaging of the deepest layers of the cartilage.

**ACKNOWLEDGMENTS**

The authors want to thank Professor Heikki Kröger, MD, PhD and Dr. Antti Joukainen, MD, PhD for their help in harvesting the osteochondral samples from the donor. Financial support from Academy of Finland (Grants: #285909, #293970, and #319440), Finnish Cultural Foundation

(Grant: #00180787), and North-Ostrobothnia regional fund of Finnish Cultural Foundation (Grant: #60172246) is also gratefully acknowledged.

**AUTHOR CONTRIBUTIONS**

ON: corresponding author, study design, drafting the paper, data acquisition and analysis; HPPL: revising the paper, data analysis; MF: revising the paper, study design, data acquisition; SSK: revising the paper, study design, data acquisition; MJT: revising the paper, data analysis; JT: revising the paper; SS: revising the paper; MJN: revising the paper, study design, data acquisition, and analysis. All authors have revised and approved this version of the manuscript.

**DATA AVAILABILITY STATEMENT**

All of the bovine data of this study are freely available for download at Zenodo (DOI: 10.5281/zenodo.3478881).

**ORCID**

- Olli Nykänen <http://orcid.org/0000-0001-7329-3463>
- Henri P. P. Leskinen <https://orcid.org/0000-0001-5043-3101>
- Mikko A. J. Finnilä <https://orcid.org/0000-0002-3348-5759>
- Mikael J. Turunen <https://orcid.org/0000-0003-1093-1178>
- Juha Töyräs <https://orcid.org/0000-0002-8035-1606>
- Simo Saarakkala <https://orcid.org/0000-0003-2850-5484>
- Mikko J. Nissi <https://orcid.org/0000-0002-5678-0689>

**REFERENCES**

1. Buckwalter JA, Mankin HJ. Instructional course lectures, The American Society of Orthopaedic Surgeons—Articular Cartilage. Part II: degeneration and osteoarthritis, repair, regeneration, and transplantation. *J Bone Joint Surg.* 1997;79:612-632.
2. Buckwalter JA, Brown TD. Joint injury, repair, and remodeling: roles in post-traumatic osteoarthritis. *Clin Orthop Relat Res.* 2004;423:7-16.
3. Bijlsma JW, Berenbaum F, Lafeber FP. Osteoarthritis: an update with relevance for clinical practice. *Lancet.* 2011;377(9783):2115-2126.
4. Burr DB, Gallant MA. Bone remodelling in osteoarthritis. *Nat Rev Rheumatol.* 2012;8(11):665-673.
5. Lories RJ, Luyten FP. The bone–cartilage unit in osteoarthritis. *Nat Rev Rheumatol.* 2011;7(1):43-49.
6. Imhof H, Breitenseher M, Kainberger F, Trattnig S. Degenerative joint disease: cartilage or vascular disease? *Skeletal Radiol.* 1997;26(7):398-403.
7. Thambyah A, Broom N. On how degeneration influences load-bearing in the cartilage–bone system: a microstructural and micromechanical study. *Osteoarthritis Cartilage.* 2007;15(12):1410-1423.
8. Suri S, Walsh DA. Osteochondral alterations in osteoarthritis. *Bone.* 2012;51(2):204-211.
9. Thambyah A, Broom N. How subtle structural changes associated with maturity and mild degeneration influence the impact-induced failure modes of cartilage-on-bone. *Clin Biomech.* 2010;25(7):737-744.
10. Burr DB. Anatomy and physiology of the mineralized tissues: role in the pathogenesis of osteoarthritis. *Osteoarthritis Cartilage.* 2004;12:20-30.
11. Kohl S, Hosalkar HS, Mainil-Varlet P, Krueger A, Buechler L, Siebenrock K. Histology of damaged acetabular cartilage in symptomatic femoroacetabular impingement: an observational analysis. *Hip Int.* 2011;21(2):154-162.
12. Bae WC, Dwek JR, Znamirovski R, et al. Ultrashort echo time MR imaging of osteochondral junction of the knee at 3 T: identification of anatomic structures contributing to signal intensity 1. *Radiology.* 2010;254(3):837-845.

13. Bae WC, Biswas R, Chen K, Chang EY, Chung CB. UTE MRI of the osteochondral junction. *Current Radiol Rep.* 2014;2(2):35.
14. Nissi MJ, Zhang J, Idiyatullin D, et al. Imaging of the osteochondral interface and deep cartilage using SWIFT. *Proc Intl Soc Mag Reson Med.*, Melbourne, Australia. 2012;p.1388.
15. Du J, Carl M, Bae WC, et al. Dual inversion recovery ultrashort echo time (DIR-UTE) imaging and quantification of the zone of calcified cartilage (ZCC). *Osteoarthritis Cartilage.* 2013;21(1):77-85.
16. Bae WC, Statum S, Zhang Z, et al. Morphology of the cartilaginous endplates in human intervertebral disks with ultrashort echo time MR imaging. *Radiology.* 2013;266(2):564-574.
17. MacKay JW, Kaggie JD, Morgan A, et al. *Ultrashort Echo Time Imaging of the Osteochondral Junction in Subjects with Knee Osteoarthritis and Age-matched Healthy Volunteers.* Paper presented at Proc Intl Soc Mag Reson Med, 2018; Paris, France.
18. Idiyatullin D, Corum C, Park JY, Garwood M. Fast and quiet MRI using a swept radiofrequency. *J Magn Reson.* 2006;181(2):342-349.
19. Wei H, Dibb R, Decker K, et al. Investigating magnetic susceptibility of human knee joint at 7 Tesla. *Magn Reson Med.* 2017;78(5):1933-1943.
20. Nykänen O, Rieppo L, Töyräs J, et al. Quantitative susceptibility mapping of articular cartilage: ex vivo findings at multiple orientations and following different degradation treatments. *Magn Reson Med.* 2018;80:2702-2716.
21. Wiener E, Pfirrmann C, Hodler J. Spatial variation in T1 of healthy human articular cartilage of the knee joint. *Br J Radiol.* 2010;83(990):476-485.
22. Nissi MJ, Lehto LJ, Corum CA, et al. Measurement of T1 relaxation time of osteochondral specimens using VFA-SWIFT. *Magn Reson Med.* 2015;74(1):175-184.
23. Wang L, Corum CA, Idiyatullin D, Garwood M, Zhao Q. T1 estimation for aqueous iron oxide nanoparticle suspensions using a variable flip angle SWIFT sequence. *Magn Reson Med.* 2013;70(2):341-347.
24. Klein S, Staring M, Murphy K, Viergever MA, Pluim JP. Elastix: a toolbox for intensity-based medical image registration. *IEEE Trans Med Imaging.* 2010;29(1):196-205.
25. Foot NC. The Masson trichrome staining methods in routine laboratory use. *Stain Technol.* 1933;8(3):101-110.
26. Kiviranta I, Jurvelin JS, Tammi M, Säämänen AM, Helminen HJ. Microspectrophotometric quantitation of glycosaminoglycans in articular cartilage sections stained with Safranin O. *Histochemistry.* 1985;82(3):249-255.
27. Pritzker KP, Gay S, Jimenez SA, et al. Osteoarthritis cartilage histopathology: grading and staging. *Osteoarthritis Cartilage.* 2006;14(1):13-29.
28. Finnilä M, Thevenot J, Aho OM, et al. Association between subchondral bone structure and osteoarthritis histopathological grade. *J Orthop Res.* 2017;35(4):785-792.
29. Rieppo J, Hyttinen MM, Halmesmaki E, et al. Changes in spatial collagen content and collagen network architecture in porcine articular cartilage during growth and maturation. *Osteoarthritis Cartilage.* 2009;17(4):448-455.
30. Yin J, Xia Y, Lu M. Concentration profiles of collagen and proteoglycan in articular cartilage by Fourier transform infrared imaging and principal component regression. *Spectrochim Acta A Mol Biomol Spectrosc.* 2012;88:90-96.
31. Dimov AV, Liu Z, Spincemaille P, Prince MR, Du J, Wang Y. Bone quantitative susceptibility mapping using a chemical species-specific signal model with ultrashort and conventional echo data. *Magn Reson Med.* 2018;79(1):121-128.
32. Ma YJ, Zhu Y, Lu X, Carl M, Chang EY, Du J. Short T2 imaging using a 3D double adiabatic inversion recovery prepared ultrashort echo time cones (3D DIR-UTE-Cones) sequence. *Magn Reson Med.* 2018;79(5):2555-2563.
33. Ma YJ, Zhao W, Wan L, et al. Whole knee joint T1 values measured in vivo at 3 T by combined 3D ultrashort echo time cones actual flip angle and variable flip angle methods. *Magn Reson Med.* 2019;81(3):1634-1644.
34. Hänninen N, Rautiainen J, Rieppo L, Saarakkala S, Nissi MJ. Orientation anisotropy of quantitative MRI relaxation parameters in ordered tissue. *Sci Rep.* 2017;7:9606.

#### SUPPORTING INFORMATION

Additional supporting information may be found online in the Supporting Information section.

**How to cite this article:** Nykänen O, Leskinen HP, Finnilä M, et al. Bright ultrashort echo time SWIFT MRI signal at the osteochondral junction is not located in the calcified cartilage. *J Orthop Res.* 2020;38:2649–2656.  
<https://doi.org/10.1002/jor.24777>